Optics Letters

Polarization-insensitive and wide-incident-angle optical absorber with periodically patterned graphene-dielectric arrays

Xiujuan Zou,[1] Gaige Zheng,[1,2,*] Jiawei Cong,[3] Linhua Xu,[1] Yunyun Chen,[1,2] and Min Lai[1]

[1]Jiangsu Key Laboratory for Optoelectronic Detection of Atmosphere and Ocean, School of Physics and Optoelectronic Engineering, Nanjing University of Information Science & Technology, Nanjing 210044, China
[2]Jiangsu Collaborative Innovation Center on Atmospheric Environment and Equipment Technology (CICAEET), Nanjing University of Information Science & Technology, Nanjing 210044, China
[3]School of Mechanical Engineering, Jiangsu University, Zhenjiang 212013, China
*Corresponding author: jsnanophotonics@yahoo.com

Received 18 October 2017; revised 27 November 2017; accepted 28 November 2017; posted 29 November 2017 (Doc. ID 309521); published 20 December 2017

A polarization-insensitive and angle-independent graphene absorber (GA) with periodically patterned grating is demonstrated. A periodic nanocavity composed of multilayer subwavelength grating and metal substrate supports a strongly localized mode inside the cavity, where the mode helps to absorb more electromagnetic waves. The proposed GA exhibits polarization-insensitive behavior and maintains the high absorption above 90% within a wide range of incident angle (more than 80°). We attribute the high absorption to the excitation of the cavity mode resonance and magnetic resonance for the transverse electric and transverse magnetic polarizations, respectively. The proposed GA has potential applications in the design of various devices, such as optical modulators or tunable absorption filters because of its remarkable angle-insensitive absorption performance.

OCIS codes: (260.5740) Resonance; (230.1950) Diffraction gratings; (230.5440) Polarization-selective devices; (230.4170) Multilayers.

https://doi.org/10.1364/OL.43.000046

Perfect light absorption [1] has attracted much attention due to its wide applications in solar energy harvesting [2,3], optical detection, sensing [4–6], and so on. Recently, various new methods to achieve good absorbers have been proposed in the fields of plasmonics and metamaterials that provide highly controllable electromagnetic (EM) response in different frequency ranges [7–14]. Among so many types of absorbers, ultra-thin absorptive films have attracted tremendous interest [15–18]. To enhance the absorption in the ultrathin absorbing layer, a resonant structure, such as a grating or a photonic crystal, can be used [12,14,19]. It is known that for ultra-thin films, the absorption rate can be up to 50% in a symmetrical environment [20,21], and such a limit can be broken by introducing symmetrical coherent illumination [22,23] or specific reflectors.

Single-atomic-layer graphene exhibits a considerable wavelength-independent absorption (≈2.3%) in an ultra-broadband wavelength region involving the visible and near-infrared (vis-NIR) spectral range, which limits its applications in optoelectronic devices [24,25]. Many approaches have been employed to improve light absorption in graphene, which can be mainly classified into two categories. One usually uses gratings or photonic crystal slabs as a resonator and an ideal metallic reflector or a dielectric Bragg reflector as a perfect mirror [26]. The other one uses two degenerate resonance modes with opposite symmetry, where each resonance can be critically coupled with the incident EM wave and is responsible for half the absorption rate [27]. However, the above two schemes are usually polarization and angle dependent and inevitably have poor tolerance for geometric parameters.

In this Letter, we propose a grating structure combined with dual pairs of graphene-dielectric thin layers deposited on a metal substrate that acts as a polarization-independent and angle-insensitive optical absorber. Structure parameters are optimized by the rigorous coupled-wave analysis (RCWA) method. To gain physical understanding of such absorption behavior, the EM field distributions at the resonance wavelengths are investigated. According to analysis, we attribute the enhanced absorption to the excitation of cavity mode resonance (CMR) and surface magnetic resonance (MR) for transverse electric (TE) and transverse magnetic (TM) polarizations, respectively. Note that it can retain a high absorption capability with the incident angle varying from 0° to 80°. Compared with those metamaterial absorbers with two-dimensional array and one-dimensional complex structures, the significance of this work is to reveal the polarization-independent and angle-insensitive absorption performance in a much simpler and flexible graphene-based grating structure.

Figure 1 presents the schematic of the proposed absorber and the propagation configuration of the incident EM wave.

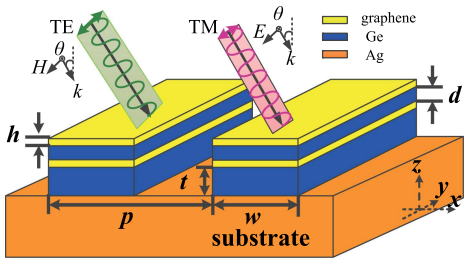

Fig. 1. Schematic of the proposed grating absorber based on a multilayer strip that consists of two pairs of graphene-Ge bilayers on Ag substrate. The structural parameters are $p = 1.18$ μm, $f = 0.45$, $h = 0.0034$ μm, $d = 0.075$ μm, and $t = 0.135$ μm.

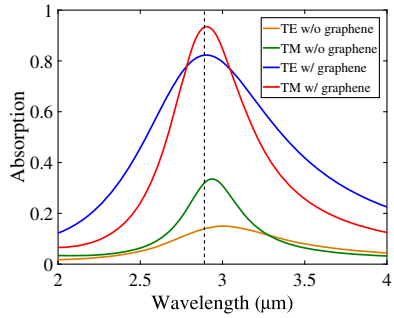

Fig. 2. Absorption spectra of the proposed grating absorber with and without graphene for TE- and TM-polarized light at normal incidence. In this case, the structural parameters of the absorber remain unchanged.

The period of grating is denoted by $p = 1.18$ μm. The ridge width of the grating is $w = f\ p$, where $f = 0.45$ is the duty cycle of the grating. The structure is finitely periodic in x direction and uniform along y direction. The material of the metal substrate is chosen as silver (Ag) whose dielectric constant is fitted by the Drude–Lorentz model [28]. The grating strips consist of dual pairs of graphene-germanium (Ge) array, which is a lossless material with high refractive index within the considered wavelength range [28,29]. The thicknesses of the top Ge grating strips and the bottom strips are $d = 0.075$ μm and $t = 0.135$ μm, respectively. The thicknesses of two graphene layers are both set as $h = 3.4$ nm, e.g., 10 times the thickness of the graphene monolayer. The graphene layer is modeled as infinitesimally thin surface with the surface conductivity σ_G calculated from Kubo formula [30]. At finite temperature, it can be divided into intra- and interband contributions:

$$\sigma_G = \sigma_G^{\text{intra}} + \sigma_G^{\text{inter}}, \tag{1}$$

$$\sigma_G^{\text{intra}} = \frac{e^2}{4\hbar}\frac{i}{2\pi}\left\{\frac{16k_BT}{\hbar(\omega + i\Gamma)}\ln\left(2\cosh\left(\frac{\mu_c}{2k_BT}\right)\right)\right\}, \tag{2}$$

$$\sigma_G^{\text{inter}} = \frac{e^2}{4\hbar}\left\{\begin{array}{l}\frac{1}{2} + \frac{1}{\pi}\arctan\frac{\hbar\omega - 2\mu_c}{2k_BT} \\ -\frac{i}{2\pi}\ln\frac{(\hbar\omega+2\mu_c)^2}{(\hbar\omega-2\mu_c)^2+(2k_BT)^2}\end{array}\right\}. \tag{3}$$

In Eqs. (2) and (3), e is the elementary charge, and $\hbar = h/2\pi$ and k_B are the reduced Planck's constant and Boltzmann constant, respectively. ω is the angular frequency. T denotes the temperature, and Γ indicates the charge carriers' scattering rate; they are chosen as 300 K and 0.1 meV, respectively.

The TM- and TE-polarized incident waves are projected on the structure from the top air-side at an angle of θ. The absorption is calculated by using the RCWA method [31]. For the calculation, a total of 101 Fourier components is used to represent the dielectric function in the grating region. To minimize the transmittance and reflectance simultaneously, impedance matching must be met. The thickness of the continuous semi-infinite metallic substrate is so thick (larger than the skin depth) that it prevents incident light from transmitting through the whole system in the infrared region. Thus, we set the transmittance of the structure as zero, and absorptivity could be calculated by $A = 1\text{-}R$, where R is the reflectivity. Figure 2 shows the absorption spectra of the absorber with and without graphene for TE and TM polarizations at normal incidence. The absorption peaks for the two polarization states are at the same resonant wavelength of 2.9 μm, but with different spectral shapes and absorption rates. For the TE polarization, the absorption spectrum possesses a typical resonant peak with a Lorenz-like line shape and a full width half-maximum (FWHM) of 1.05 μm. Under the TM polarization, the absorption spectrum is a Gaussian-like line shape with a narrower FWHM of 0.59 μm. The graphene absorptivity at 2.9 μm is calculated to be 67.3% (60.5%) for TE (TM) polarization, where the proposed absorber absorptivity is 82.3% (93.5%) and grating absorptivity without graphene is 15% (33%). In addition, the off-resonance absorption of the TM polarization is lower than that of the TE polarization.

In order to understand the physical mechanisms that give rise to enhanced absorption at the same wavelength for TE and TM polarizations, the EM field distributions corresponding to the absorption peaks are depicted in Fig. 3. For TE-polarized light, the only three non-zero field components are E_y, H_x, and H_z with a coordinate system oriented as in Fig. 1. For TM-polarized light, the three non-zero field components are E_x, H_y, and E_z. Obviously, the TE- and

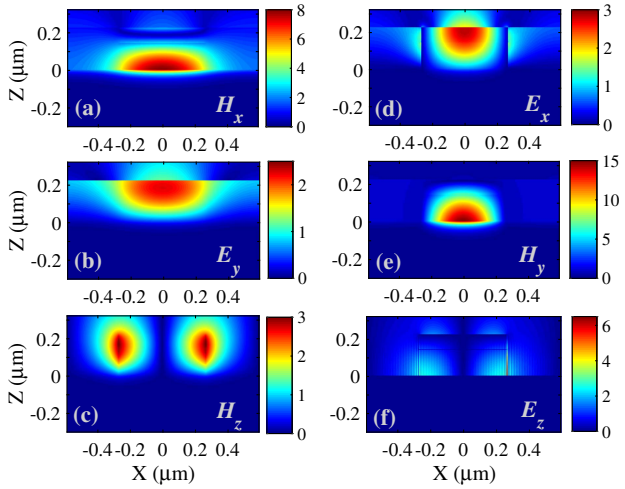

Fig. 3. Calculated electromagnetic field distributions of the absorber at the resonant wavelength of 2.9 μm at normal incidence for TE-polarized light (a)–(c) and TM-polarized light (d)–(f).

TM-polarized waves are absorbed in different components of the structure.

The field patterns associated with the enhanced absorption at $\lambda \approx 2.9$ μm for TE polarization are plotted in Figs. 3(a)–3(c). It is shown that the field is strongly confined within the slits of Ge and depicts a typical feature of cavity resonance. The resonant wavelength of an ideal cavity under TE polarization is given as [32]

$$\lambda_{\mathrm{mn}} = \frac{2\sqrt{\varepsilon}}{\sqrt{(m/(p-w))^2 + (n/(2h+d+t))^2}}, \quad m, n = 1, 2, \ldots, \tag{4}$$

where ε is the dielectric constant of grooves. Equation (4) is established on the basis of the theory of a planar-mirror waveguide. It clearly shows that λ_{mn} can be controlled by a change of d, t, h, and p.

As presented in Fig. 3(a), the component H_x is strongly localized essentially in the bottom Ge grating strips, and some energy penetrates into the Ag substrate. The electric field is mostly concentrated in the top Ge grating and leaks into the slits between the neighboring strips, which indicates that the resonance occurs at this layer, as shown in Fig. 3(b). The electric field distribution of E_y is analogous to the cavity mode with $m = n = 1$. However, the intensity of EM fields for TM polarization is larger than that of the TE-polarized state. It is found that there is a large magnetic field enhancement mainly localized in the Ge layers and dielectric–metal interface, as shown in Fig. 3(e). The physical mechanism responsible for the near-perfect absorption of the TM-polarized light can be attributed to MR, which can be explained by the equivalent LC circuit model [33–35]. By zeroing the total impedance, we can obtain the predicted resonant wavelength of 2.9 μm. The components H_z and E_z are essentially confined in the lateral edge of the grating ridges, where H_z is mainly localized in the top Ge strips, and E_z is in the bottom Ge strips, which can be seen in Figs. 3(c) and 3(f).

The wide-angle feature is very important for practical applications of absorbers, and the absorption rates should be retained high enough for a wide range of incident angle. Thus, we regard the independence of angle of incidence as a figure of merit. In Figs. 4(a) and 4(b), the absorption spectra as a function of angle at the resonant wavelength of 2.9 μm is first simulated so as to clearly present the wide angle range of absorption for TE and TM polarizations. As displayed, it is above 90% (80%) for incident angles up to 73° (78°) for TE polarization, and above 90% (80%) for angles up to 81° (84°) for TM polarization. Furthermore, the absorption as a function of wavelength and the angle of incidence is simulated in order to analyze the angle independence and the shift of resonant wavelength, as shown in Figs. 4(c) and 4(d). It is found that there is an absorption band near the wavelength of 3 μm with the increasing angle for both polarized lights. For angles from 0° to 80°, the absorption peaks are all above 80%. However, the central wavelength increases by 51 nm for TE polarization and decreases by 2 nm for TM polarization, which shows a red and blue shift of absorption peaks, respectively. It should be noted that the wavelength shifts are both within the line width of the absorption peak, so it can be concluded that the graphene-based grating absorber has strong angle independence. The absorption is much weaker at other

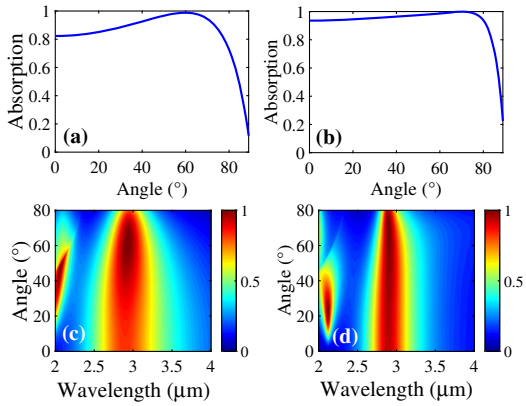

Fig. 4. Absorption spectra of the absorber as a function of incident angle at the resonant wavelength of 2.9 μm for TE (a) and TM (b) polarizations. Absorption maps as a function of incidence angle and wavelength for TE (c) and TM (d) polarizations, respectively. Other parameters are the same as those in Fig. 2.

wavelengths, though there is an additional absorption band at a smaller wavelength for a very short range of incident angle.

To optimize the proposed structural performance of the absorber, we investigate the relationship between the absorption and the geometric parameters. In Fig. 5, we show the absorption maps as a function of wavelength and d, t, as well as p. The basic parameters for all plots are obtained from Fig. 1, unless otherwise specified. It can be found that d cannot be too large, and t cannot be too small so as to obtain the wavelength-independent high absorption for different polarizations. It is impossible to achieve high absorption peaks with the same wavelength for the two polarizations when d and t are denoted larger than the ranges discussed.

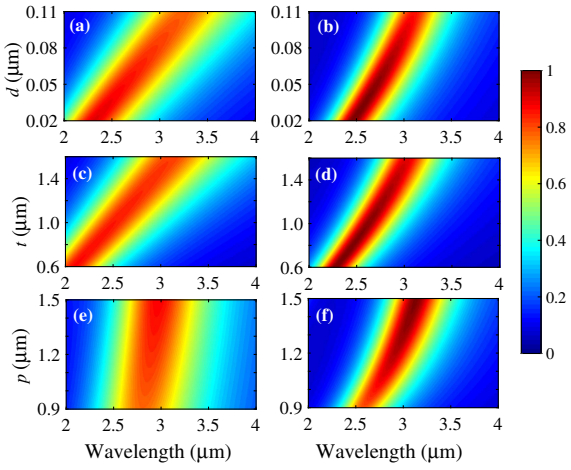

Fig. 5. Absorption maps as a function of wavelength and thickness of the top dielectric layer Ge, thickness of the bottom dielectric layer Ge, and grating period for TE polarization (a), (c), (e) and TM polarization (b), (d), (f). The structural parameters are: $\theta = 0°$, $p = 1.18$ μm, $w = 0.45$ μm, $h = 0.0034$ μm, $d = 0.075$ μm, $t = 0.135$ μm, and $s = 0.2$ μm. In (a) and (b), d is varied from 0.02 to 0.11 μm, in (c) and (d), t is varied from 0.6 to 1.6 μm, and in (e) and (f), p is varied from 0.9 to 1.5 μm.

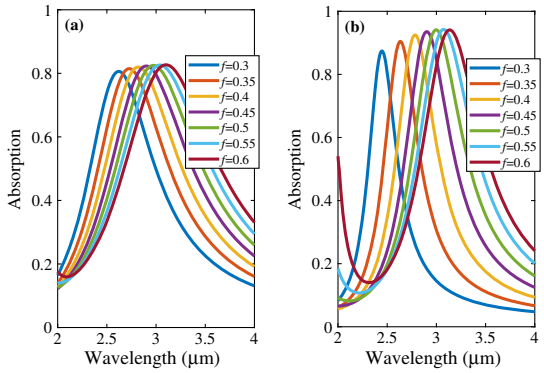

Fig. 6. Absorption spectra as a function wavelength and duty cycle f for TE (a) and TM (b) polarization. Duty cycle is varied from 0.3 to 0.6, but other parameters remain unchanged.

For the sake of enhancing the absorption, it is undesirable for high reflection at the air–grating interface. Thus, the reflection can be reduced, and the transmission and can be enhanced by employing grating with a large grating period and duty cycle. Furthermore, Figs. 5(e) and 5(f) demonstrate that the grating period should be large so as to achieve high absorption whose peak is almost independent with the grating period for TE polarization. In Fig. 6, the effect of duty cycle on the enhanced absorption is studied, which manifests that FWHM of the absorption peaks expands with the increase of the duty cycle. Furthermore, the resonant wavelengths become the same for TE and TM polarizations when the duty cycle is denoted by $f = 0.45$.

In conclusion, the absorption effects of the proposed grating-based absorber with periodically patterned graphene strips are discussed. The wide-angle independence of the absorber under TE and TM polarizations is achieved. The mechanisms of the angle-independent graphene absorber (GA) are illustrated by investigating the field distributions under the above two polarizations. It is found that the high absorption of the absorber are attributed to CMR for TE polarization and MR for TM polarization, respectively. The absorption rate and the resonant wavelength can be tuned by varying the structural parameters. The proposed GA with periodically patterned subwavelength gratings may have potential applications in graphene-based optoelectronic devices, such as optical modulators and tunable absorption filters.

Funding. National Natural Science Foundation of China (NSFC) (41675154, 61203211); Natural Science Foundation of Jiangsu Province (BK20141483); Jiangsu 333 High-Level Talent Cultivation Program (BRA2016425); Innovation Project of Graduate Education in Jiangsu Province (KYCX17_0898); Six Major Talent Peak Expert of Jiangsu Province (2015-XXRJ-014).

REFERENCES

1. N. I. Landy, S. Sajuyigbe, J. J. Mock, D. R. Smith, and W. J. Padilla, Phys. Rev. Lett. **100**, 207402 (2008).
2. H. A. Atwater and A. Polman, Nat. Mater. **9**, 205 (2010).
3. Y. Cui, Y. He, Y. Jin, F. Ding, L. Yang, Y. Ye, S. Zhong, Y. Lin, and S. He, Laser Photon. Rev. **8**, 495 (2014).
4. K. Bhattarai, Z. Ku, S. Silva, J. Jeon, J. Kim, S. Lee, A. Urbas, and J. Zhou, Adv. Opt. Mater. **3**, 1779 (2015).
5. F. Frascella, S. Ricciardi, P. Rivolo, V. Moi, F. Giorgis, E. Descrovi, F. Michelotti, P. Munzert, N. Danz, L. Napione, M. Alvaro, and F. Bussolino, Sensors **13**, 2011 (2013).
6. W. H. Yang, C. Zhang, S. Sun, J. Jing, Q. Song, and S. Xiao, Nanoscale **9**, 8907 (2017).
7. X. Liu, T. Starr, A. F. Starr, and W. J. Padilla, Phys. Rev. Lett. **104**, 207403 (2010).
8. H.-T. Chen, J. Zhou, J. F. O'Hara, F. Chen, A. K. Azad, and A. J. Taylor, Phys. Rev. Lett. **105**, 073901 (2010).
9. D. Ye, Z. Wang, K. Xu, H. Li, J. Huangfu, Z. Wang, and L. Ran, Phys. Rev. Lett. **111**, 187402 (2013).
10. K. Bhattarai, S. Silva, K. Song, A. Urbas, S. J. Lee, Z. Ku, and J. Zhou, Sci. Rep. **7**, 10569 (2017).
11. B. S. Tung, B. X. Khuyen, Y. J. Kim, V. D. Lam, K. W. Kim, and Y. P. Lee, Sci. Rep. **7**, 11507 (2017).
12. B. Zhao and Z. M. Zhang, Int. J. Heat Mass Transfer **106**, 1025 (2017).
13. H. Lu, X. Gan, D. Mao, Y. Fan, D. Yang, and J. Zhao, Opt. Express **25**, 21630 (2017).
14. B. Zhao and Z. M. Zhang, Opt. Express **25**, 7791 (2017).
15. M. Serhatlioglu, S. Ayas, N. Biyikli, A. Dana, and M. E. Solmaz, Opt. Lett. **41**, 1724 (2016).
16. K. Arik, S. Abdollahramezani, and A. Khavasi, Plasmonics **12**, 393 (2017).
17. Y. S. Fan, C. C. Guo, Z. H. Zhu, W. Xu, F. Wu, X. D. Yuan, and S. Q. Qin, Opt. Express **25**, 13079 (2017).
18. S. S. Mirshafieyan, T. S. Luk, and J. Guo, Opt. Mater. Express **6**, 1032 (2016).
19. C. C. Guo, Z. H. Zhu, and X. D. Yuan, Adv. Opt. Mater. **4**, 1955 (2016).
20. S. Thongrattanasiri, F. H. L. Koppens, and F. D. Abajo, Phys. Rev. Lett. **108**, 047401 (2012).
21. J. R. Piper and S. Fan, ACS Photon. **1**, 347 (2014).
22. H.-T. Chen, Opt. Express **20**, 7165 (2012).
23. J. Luo, S. C. Li, B. Hou, and Y. Lai, Phys. Rev. B **90**, 165128 (2014).
24. K. S. Novoselov, V. I. Fal'ko, L. Colombo, P. R. Gellert, M. G. Schwab, and K. K. Schwab, Nature **490**, 192 (2012).
25. R. R. Nair, P. Blake, A. N. Grigorenko, K. S. Novoselov, T. J. Booth, T. Stauber, N. M. Peres, and A. K. Geim, Science **320**, 1308 (2008).
26. S. Lee, T. Q. Tran, H. Heo, M. Kim, and S. Kim, Sci. Rep. **7**, 4760 (2017).
27. J. R. Piper, V. Liu, and S. Fan, Appl. Phys. Lett. **104**, 251110 (2014).
28. E. D. Palik, *Handbook of Optical Constants of Solids* (Academic, 1998).
29. J. H. Lee, E. K. Lee, and W. J. Joo, Science **344**, 286 (2014).
30. L. A. Falkovsky and S. S. Pershoguba, Phys. Rev. B **76**, 153410 (2007).
31. P. Lalanne and G. M. Morris, J. Opt. Soc. Am. A **13**, 779 (1996).
32. Y. Lu, M. H. Cho, Y. Lee, and J. Y. Rhee, Appl. Phys. Lett. **93**, 061102 (2008).
33. L. P. Wang, A. M. Haider, and Z. M. Zhang, J. Quant. Spectrosc. Radiat. Transfer **132**, 52 (2014).
34. S. Abdollahramezani, K. Arik, and A. Khavasi, Opt. Lett. **40**, 5239 (2015).
35. S. Abdollahramezani, K. Arik, and S. Farajollahi, Opt. Lett. **40**, 5383 (2015).